Swirling of Viscous Fluid Threads in Microchannels

Thomas Cubaud and Thomas G. Mason*

Department of Chemistry and Biochemistry, Department of Physics and Astronomy, California NanoSystems Institute, University of California, Los Angeles, California 90095, USA

(Received 6 June 2006; published 28 June 2007)

Viscous threads that are swept along in the flow of a less viscous miscible liquid can break up into viscous swirls. We experimentally investigate the evolution of miscible threads that flow off center in microchannels. Thin threads near the walls of a straight square channel become unstable to shear-induced disturbances. The amplification of the undulations transverse to the flow direction ultimately causes the threads to break up and form an array of individual viscous swirls, the miscible counterparts of droplets. This swirling instability provides a means for passively producing discrete diffusive microstructures in a continuous flow regime.

DOI: 10.1103/PhysRevLett.98.264501 PACS numbers: 47.15.Fe, 47.20.−k, 47.60.+i, 83.50.−v

The dynamics and coupling between miscible liquids having different viscosities and velocity fields can lead to a rich array of morphologies and instabilities. Although numerous studies have addressed the stability of viscous-stratified flows [1–5] and the viscous fingering that results from miscible displacements of a liquid into another [6–8], relatively less is known about the behavior of viscous threads in miscible environments [9]. This is due at least in part to the transient and short-lived nature of miscible viscous structures, since initially segregated liquids will ultimately evolve into a homogenous mixture due to intermolecular diffusion. For short intervals of time τ, slender viscous structures can exhibit dynamic responses to stress resembling those of elastic solids [10–13]. In this situation, the fluid displays ''intermediate'' properties between a fluid having a viscosity η and an amorphous solid having a modulus of rigidity μ. The relationship between the orders of magnitude of these parameters is $\mu \sim \eta/\tau$ [14]. By analogy to the term ''elastica,'' referring to slender elastic structures, slender viscous structures are sometimes called ''viscida'' [15].

Microfluidic systems offer a fast and compact means of investigating the production of regular patterns of fluids far from equilibrium [16–19]. Microfluidic investigations of viscous threads flowing in a less viscous miscible liquid in diverging slit microchannels have revealed a transition from periodic to chaotic folding [20]. The rupturing of a continuous liquid phase into discrete elements represents an important class of instabilities in fluid mechanics. Threads and jets of one liquid in another immiscible fluid can undergo a capillary instability and break up into droplets through amplification of varicose undulations by surface tension [21,22]. By contrast, in the absence of surface tension, the ability to rupture viscous threads into discrete elements would open up a wide range of possibilities for structuring flows.

Here, we investigate the dynamics of two viscous threads surrounded by a less viscous miscible liquid that coflow in straight square microchannels. We have constructed a silicon-based microfluidic module with two symmetrical square hydrodynamic focusing cross channels in series [Fig. 1(a)]. The module is a sandwich of a silicon wafer of thickness $h = 100$ μm that has been etched through and anodically bonded between borosilicate glass plates on both sides. Two miscible silicone oils (polydimethylsiloxane) having viscosities $\eta_1 = 6$ cP ($L1$) and $\eta_2 = 500$ cP ($L2$) are chosen, so diffusion and buoyancy do not significantly alter the threads as they traverse the channel [20].

In the first cross channel, the less viscous oil is injected with a volume flow rate Q_1, and the more viscous oil is injected from the two side channels at a total rate Q_2. The flow adopts a steady-state configuration consisting of a central strip of $L1$ in contact with the upper and lower walls and bounded by $L2$ on either side. In the second

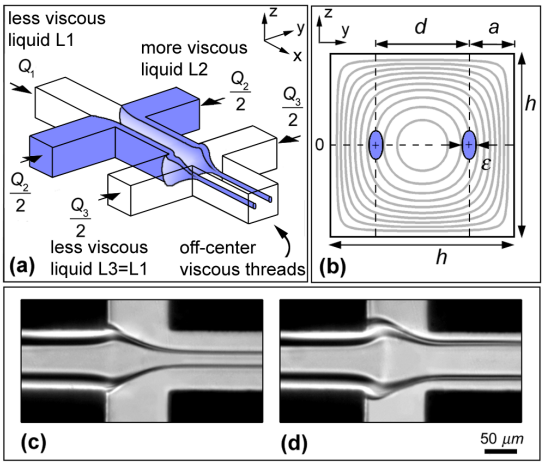

FIG. 1 (color online). Forming two off-center viscous threads. (a) Two-step hydrodynamic focusing in square channels. The less viscous liquids $L1$ and $L3$ ($\eta_1 = \eta_3 = 6$ cP) are identical and injected at volume flow rates, Q_1 and Q_3, respectively; the more viscous liquid $L2$ ($\eta_2 = 500$ cP) is injected at Q_2 and forms two threads. (b) Schematic cross-sectional contour plot of the mean flow velocity in the square outlet microchannel. (c),(d) Experimental micrographs with flow rates ($\mu l/\min$): (c) $Q_1 = 20$, $Q_2 = 1$, $Q_3 = 60$; (d) $Q_1 = 20$, $Q_2 = 1$, $Q_3 = 7$.

cross-channel, the less viscous oil ($L3 = L1$) having $\eta_3 = \eta_1$ is injected from the two side channels at a total rate Q_3 and impinges on this stratified flow. The two layers of the more viscous oil detach from the walls and become completely surrounded by less viscous oil, yielding two symmetrical threads swept along in the flow of $L1$ and $L3$. The lubrication of the threads by the less viscous oil represents a configuration that reduces dissipation. The threads flow off-center in the straight square channel having length $L = 50h$ and are initially characterized by their separation d and their width ε. Since buoyancy is negligible, the threads are assumed to travel downstream in the median plane of the square channel at $z = 0$. Therefore, their separation d and their position relative to the sidewalls, $a = (h - d)/2$, are solely functions of the coordinate y. Thin threads are formed when $Q_2 \ll Q_1 + Q_3$, corresponding to $\varepsilon \ll h$. In this asymptotic regime, we assume that the threads do not significantly perturb the mean flow field, $\boldsymbol{U} = U(y, z)\boldsymbol{x}$, generated by $L1$ and $L3$ [Fig. 1(b)]. In the second cross channel, the flow structure displays characteristic "horns" [Figs. 1(c) and 1(d)] as the two layers of $L2$ detach from the walls due to the cross flow of $L3$. All flows are strongly laminar since the Reynolds numbers are $\mathrm{Re}_1 = \rho_1(Q_1 + Q_3)/(\eta_1 h) < 1$ for $L1$ and $L3$ and $\mathrm{Re}_2 = \rho_2 Q_2/(\eta_2 \varepsilon) < 10^{-2}$ for $L2$, where ρ_i is the density associated with the liquid i. Hence, the threads have well-defined shapes and positions with negligible drift velocities, and the flow is fully developed after an entrance length of approximately h.

We have measured d as a function of Q_1/Q_3 for different values of Q_1/Q_3 [Fig. 2]. The laminar flow of the identical liquids $L1$ and $L3$ forms a virtual "interface" at which the threads are localized. The theoretical width of the focused stream of $L1$, $d^*(Q_1/Q_3)$, can be simply computed by integrating the Fourier series of $U(y, z)$ in the square channel [23] between $z = -h/2$ and $h/2$ and between $y = -d^*/2$ and $d^*/2$ in order to obtain $Q_1(d^*)$ for d^* ranging between 0 and h. Since the total flow rate, $Q_{\mathrm{tot}} = Q_1 + Q_3$, does not depend on d^*, one can write $Q_1/Q_3 = (Q_{\mathrm{tot}}/Q_1 - 1)^{-1}$ and then plot d^*/h versus Q_1/Q_3 [Fig. 2]. Although the trend for the computed d^* is very similar to the experimental data for $d(Q_1/Q_3)$, it slightly underestimates d. For reference, we also plot the analytical solution of the Stokes equations, $d^{**}/h = [1 + (Q_1/Q_3)^{-1}]^{-1}$, for a plane geometry [24]. The measured d lies in a narrow band between the lower and upper bounds defined, respectively, by d^* and d^{**} [Fig. 2]. The threads are swept along by a velocity field that can be estimated by the parabolic (Poiseuille) flow: $U(y, z = 0) \approx U_{\mathrm{max}}[1 - (2y/h)^2]$ with $U_{\mathrm{max}} = 2.1(Q_1 + Q_2 + Q_3)/h^2$, where the constant 2.1 is due to the channel's square cross section. Given the large viscosity contrast, $\eta_2 \gg \eta_1$, the velocity field within the threads is nearly uniform with a velocity U_2 which approximately matches $U(y = d/2, z = 0)$. To characterize the thread's cross-sectional shape, we compare the measured ε to the diameter of a cylindrical thread ε_c, which can be estimated by mass conservation:

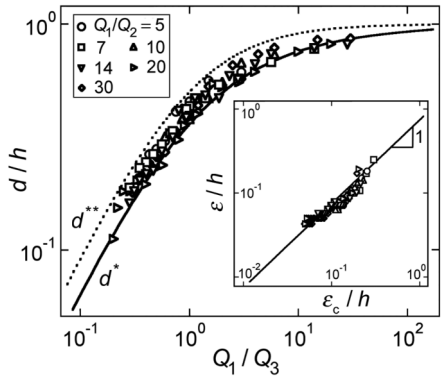

FIG. 2. Thread separation d/h versus the flow rate ratio Q_1/Q_3. Numerical computation of the position of the interface between $L1$ and $L3$ predicts a separation d^* (solid line). An analytic equation assuming a plane geometry yields a prediction d^{**} (dashed line). Inset: Measured thread width ε/h compared to the diameter of a thread of circular cross section ε_c/h.

$\varepsilon_c \approx \{2Q_2/[\pi U_{\mathrm{max}}(1 - (d/h)^2)]\}^{1/2}$ [Fig. 2, inset]. We find empirically that $\varepsilon \approx 0.75\varepsilon_c$, which suggests the threads would rather assume an elliptical cross-sectional shape with $\varepsilon = \varepsilon_y$ being the minor axis and ε_z being the major axis. In order to conserve the mass flux inside the threads, the thread cross-sectional area follows $\pi\varepsilon_y\varepsilon_z/4 = \pi\varepsilon_c^2/4$ yielding $\varepsilon_y \approx (0.75)^2\varepsilon_z$. This corresponds typically to an ellipse with an aspect ratio of 2 between the major and the minor axis. By adjusting the flow rates, ε and d can be set independently, thereby permitting a systematic exploration of the evolution and coupling of off-axis viscous threads in channel flows.

By contrast to a single nondiffusive thread flowing stably in the center of the microchannel, off-axis threads can become unstable [Fig. 3(a)]. As the threads flow downstream, sinuous perturbations with a characteristic wavelength λ develop in the y direction [Fig. 3(b)]. These disturbances are accompanied by a bending and a stretching of the thread and are amplified into a continuous wavelike pattern. Eventually, each thread breaks up into a linear array of discrete viscous swirls. Two widely separated threads are decoupled and the growth of perturbations can occur at different locations in the channel. Empirically, we find that the slenderness ratio of the perturbations λ/ε, analogous to the most unstable aspect ratio, increases with the distance $a = (h - d)/2$ from the nearest sidewall [Fig. 3(c)]. We interpret this instability as resulting from the competition between the torque generated by the mean flow on the threads and their dynamic viscous rigidity. According to the slender-body theory for Stokes flows [25,26], the drag force acting on a slender spheroid of length λ and diameter ε can be expressed to first order as $F_D \approx 2\pi\eta_1\lambda U/[\ln(\lambda/\varepsilon) - 0.8]$. Since our threads are initially continuous, we neglect end effects [27] and use $F_D \approx 2\pi\eta_1\lambda U$ for the drag force acting on a finite section of length λ of an infinite cylindrical thread, a shape we shall now assume to simplify the analysis. The difference

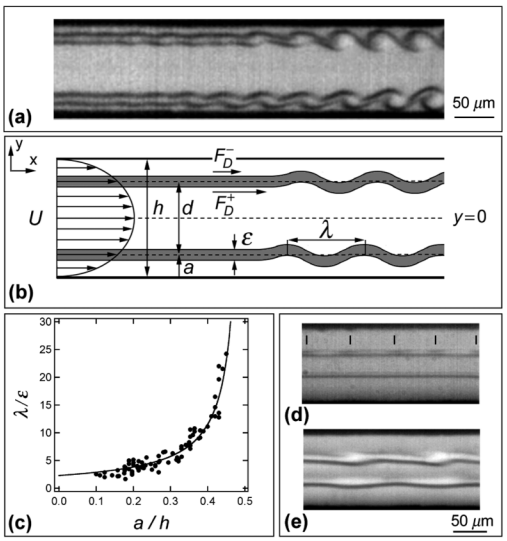

FIG. 3. Shear-induced destabilization of viscous threads. (a) Disturbances are amplified as the threads propagate downstream (from left to right). Flow rates (μl/min): $Q_1 = 40$, $Q_2 = 5$, $Q_3 = 20$. (b) Schematic diagram of the onset of swirling instability. (c) Slenderness ratio λ/ε versus distance to the sidewall a/h. Solid line: $\lambda/\varepsilon = 2.8 \times 10^{-2}(\eta_2/\eta_1)/(1-2a/h)$. (d),(e) Large slenderness ratios: (d) $\lambda/\varepsilon \approx 9.6$, $Q_1 = 10$, $Q_2 = 1$, $Q_3 = 30$; (e) $\lambda/\varepsilon \approx 7.8$, $Q_1 = 10$, $Q_2 = 5$, $Q_3 = 40$.

in drag forces on either side of a given thread section, at positions $y^{\pm} = (d \pm \varepsilon)/2$, produces a torque $T = (\varepsilon/2)(F_D{}^{+} - F_D{}^{-}) \approx 4\pi\eta_1\lambda d\varepsilon^2 U_{\max}/h^2$. According to the viscous-elastic analogy, the dynamic Young's modulus of the threads scales as $E \sim 3\eta_2/\tau$ [11], where $t \sim h/(2U_{\max})$ is the characteristic (short) time scale associated with the flow. The bending moment K associated to the threads is $K = EI/R$, where $I = (\pi/4)(\varepsilon/2)^4$ is the moment of inertia of a cylindrical thread and R is the radius of curvature of the centerline [14]. Since the viscous torque initially acts over a distance $\varepsilon/2$ from the thread centerline, the typical radius of curvature is estimated to be $R \sim \varepsilon/2$, which yields to the following critical bending moment: $K \approx (3\pi/16)\eta_2 U_{\max}\varepsilon^3/h$. As the torque acts on the thread, the thread begins to rotate and bend around a series of nodes. The spacing between the nodes, λ, can be estimated by balancing the moments at the onset of the instability: $T \approx K$. We obtain a relationship for the slenderness ratio of the perturbations: $\lambda/\varepsilon \approx C(\eta_2/\eta_1)/(1-2a/h)$, with the constant $C = 3/64 \approx 4.7 \times 10^{-2}$. This relation diverges as the thread approaches the center of the channel where the velocity gradient vanishes. We fit the measured aspect ratio to $C_{\exp}(\eta_2/\eta_1)(1-2a/h)$ [Fig. 3(c)], where $C_{\exp}$ is the only adjustable parameter and we find $C_{\exp} = 2.8 \times 10^{-2}$, yielding $C/C_{\exp} \approx 1.7$. Since our approximate model is based on scaling arguments for T and K, it yields good qualitative agreement, on the order of magnitude of the experiment. Taking into account the elliptical shape of the threads does not significantly change C. The scatter in the data for small a/h gives evidence of more complex dynamic processes occurring near the walls [Fig. 3(a)] as opposed to near the channel axis [Figs. 3(d) and 3(e)].

The deformation morphologies of the threads as the instability develops depend on λ/ε [Figs. 4(a)–4(c)]. A thread's centerline evolves from initial sinuous undulations towards oblique wavelike shapes. For large λ/ε [Fig. 4(a)], a section of a thread rolls up on itself, similar to what has been observed for long flexible filaments [28]. For smaller λ/ε [Figs. 4(b) and 4(c)], the peaks in the high shear region grow by collecting liquid into central "bulbs" at the expense of the regions in between them, which thin and resemble "tails." Eventually, the tails become so thin that they disappear as the molecules diffuse into the surrounding oil, thereby separating neighboring swirls. Initially, the average swirl diameter D can be estimated by mass conservation to scale as $D \sim (\lambda\varepsilon^2)^{1/3}$. After detaching from one another, isolated swirls gain angular momentum and rotate [Fig. 4(d)], as expected for objects in a shear field [29,30]. Small fluctuations in a swirl's position toward the center of the channel can induce a local increase of its velocity and cause neighboring swirls to pair. These swirls are heterogeneous and ephemeral structures; eventually diffusion causes them to disappear.

While we also observe the swirling instability with a single off-center thread, the system formed by two initially symmetrical threads provides access to a wider range of dynamical behaviors. In particular, we identify two regimes: one corresponding to the decoupling of thin threads near the walls and the other corresponding to the coupling of thick threads near the center. The hydrodynamic coupling of the threads is best revealed in a diverging slit

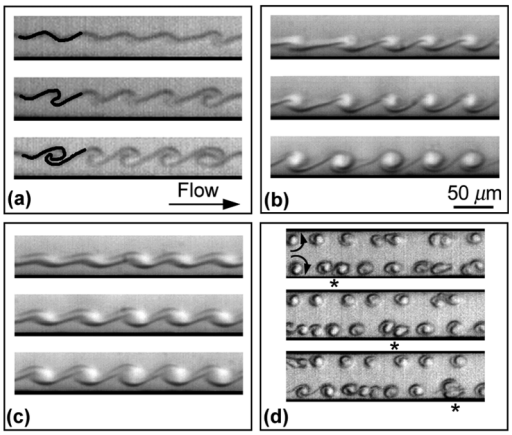

FIG. 4. Time series (from top to bottom in each panel) of thread deformations and swirl motion. (a)–(c) Single thread near the lower sidewall (thread's reference frame). (a) $\lambda/\varepsilon \approx 5$, $\Delta t = 4 \times 10^{-3}$ s), flow rates (μl/min): $Q_1 = 20$, $Q_2 = 2$, $Q_3 = 20$. (b) $\lambda/\varepsilon \approx 4.1$, $\Delta t = 3 \times 10^{-3}$ s, $Q_1 = 20$, $Q_2 = 4$, $Q_3 = 20$. (c) $\lambda/\varepsilon \approx 3.8$, $\Delta t = 3 \times 10^{-3}$ s, $Q_1 = 15$, $Q_2 = 3$, $Q_3 = 15$. (d) Swirls rotate (arrows) in opposite directions as they move downstream (channel's reference frame), $Q_1 = 20$, $Q_2 = 1$, $Q_3 = 20$ ($\Delta t = 2 \times 10^{-3}$ s). Neighboring swirls can pair (*).

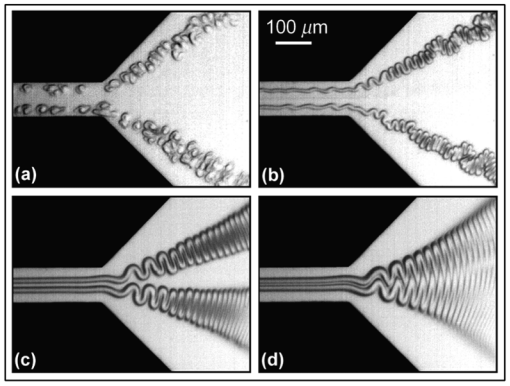

FIG. 5. Crossover between the swirling instability and the phase-locked multiple folding instability of two threads in a diverging slit microchannel. (a) In the decelerating flow, swirls deform, pile up, and merge to form heterogeneous streams, flow rates (μl/min): $Q_1 = 20$, $Q_2 = 1$, and $Q_3 = 20$. (b) Destabilized thin threads, $Q_1 = 20$, $Q_2 = 5$, and $Q_3 = 40$. (c),(d) Coupled threads, $Q_2 = 5$ and $Q_3 = 15$: (c) phase-locked multiple folding, $Q_1 = 5$; (d) intermingling folding pattern, $Q_1 = 1$.

microchannel [Fig. 5]. At the divergence, swirls pile up and merge with each other forming heterogeneous streams [Fig. 5(a)]. As d decreases, thin threads are still subject to shear-induced disturbances but remain continuous; at the divergence, they form irregular decoupled folding patterns [Fig. 5(b)]. Thick proximate threads remain stable near the center and fold in phase in the divergence [Fig. 5(c)]. The phase locking of nearby threads resembles the coupling between flexible filaments in a flowing fluid [31] and jets descending into density-stratified surroundings [32]. For $d < \varepsilon$, although threads are distinct from one another, the switchbacks of folding interpenetrate [Fig. 5(d)]. Eventually, as $Q_1 \rightarrow 0$, we recover the symmetric folding of a single thread [20].

Although the swirling instability we observe presents some similarities with the inertially dominated Kelvin-Helmholtz instability [21], it is more closely related to shear-induced buckling of viscida [33] and elastica [28]. Linear and nonlinear stability analyses, as well as numerical simulations, would provide more quantitative insights into the swirling instability. Our study demonstrates the possibility of forming and controlling the size and the shape of discrete diffusive viscous elements at the microscale.

The authors thank J. McTague for supporting this work and C.-M. Ho for the use of the high speed camera. We have enjoyed discussions with R. Bruinsma and A. Levine.

*Author to whom correspondence should be addressed. mason@chem.ucla.edu.

[1] C. S. Yin, J. Fluid Mech. **27**, 337 (1967).
[2] C. H. Li, Phys. Fluids **12**, 2473 (1969).
[3] C. E. Hickox, Phys. Fluids **14**, 251 (1971).
[4] B. Khomami and K. C. Su, J. Non-Newtonian Fluid Mech. **91**, 59 (2000).
[5] Q. Cao, A. L. Ventresca, K. R. Sreenivas, and A. K. Prasad, Can. J. Chem. Eng. **81**, 913 (2003).
[6] J.-C. Bacri, D. Salin, and R. Wouméni, Phys. Rev. Lett. **67**, 2005 (1991).
[7] E. Lajeunesse, J. Martin, N. Rakotomalala, D. Salin, and Y. C. Yortsos, J. Fluid Mech. **398**, 299 (1999).
[8] R. Balasubramaniam, N. Rashidnia, T. Maxworthy, and J. Kuang, Phys. Fluids **17**, 052103 (2005).
[9] R. W. Griffiths and J. S. Turner, Geophys. J. **95**, 397 (1988).
[10] R. da Silveira, S. Chaieb, and L. Mahadevan, Science **287**, 1468 (2000).
[11] A. Boudaoud and S. Chaieb, Phys. Rev. E **64**, 050601(R) (2001).
[12] N. M. Ribe, J. Fluid Mech. **433**, 135 (2001).
[13] M. Maleki, M. Habibi, R. Golestanian, N. M. Ribe, and D. Bonn, Phys. Rev. Lett. **93**, 214502 (2004).
[14] L. D. Landau and E. M. Lifshitz, *Theory of Elasticity* (Pergamon, Oxford, 1986).
[15] J. D. Buckmaster, A. Nachan, and L. Ting, J. Fluid Mech. **69**, 1 (1975).
[16] H. A. Stone, A. D. Stroock, and A. Ajdari, Annu. Rev. Fluid Mech. **36**, 381 (2004).
[17] T. Cubaud, M. Tatineni, X. Zhong, and C.-M. Ho, Phys. Rev. E **72**, 037302 (2005).
[18] T. M. Squires and S. R. Quake, Rev. Mod. Phys. **77**, 977 (2005).
[19] J. Atencia and D. J. Beebe, Nature (London) **437**, 648 (2005).
[20] T. Cubaud and T. G. Mason, Phys. Rev. Lett. **96**, 114501 (2006).
[21] S. Chandrasekhar, *Hydrodynamic and Hydromagnetic Stability* (Dover, New York, 1981).
[22] J. Eggers, Rev. Mod. Phys. **69**, 865 (1997).
[23] F. M. White, *Viscous Fluid Flow* (McGraw-Hill, New York, 1991).
[24] Z. Wu and N.-T. Nguyen, Sens. Actuators B Chem. **107**, 965 (2005).
[25] G. K. Batchelor, J. Fluid Mech. **44**, 419 (1970).
[26] R. G. Cox, J. Fluid Mech. **44**, 791 (1970).
[27] A. M. D. Davis and H. Brenner, Phys. Fluids **13**, 3086 (2001).
[28] O. L. Forgacs and S. G. Mason, J. Colloid Sci. **14**, 473 (1959).
[29] T. G. M. van de Ven, *Colloidal Hydrodynamics* (Academic, San Diego, 1989).
[30] H. Liu, H. H. Bau, and H. Hu, Phys. Fluids **16**, 998 (2004).
[31] J. Zhang, S. Childress, A. Libchaber, and M. Shelley, Nature (London) **408**, 835 (2000).
[32] C. Dombrowski, B. Lewellyn, A. I. Pesci, J. M. Restrepo, J. O. Kessler, and R. E. Goldstein, Phys. Rev. Lett. **95**, 184501 (2005).
[33] S. M. Suleiman and B. R. Munson, Phys. Fluids **24**, 1 (1981).